Acta Cryst. (1977). A33, 605–609

A Method of Determining the Order Parameter from Thickness Fringes in Electron Micrographs

BY CHIKEN KINOSHITA, TOSHIO MUKAI AND SADAKICHI KITAJIMA

Department of Nuclear Engineering, Faculty of Engineering, Kyushu University, Fukuoka 812, *Japan*

(*Received* 7 *October* 1976; *accepted* 27 *December* 1976)

A method of determining the long-range order parameter S in alloys with a high accuracy from thickness fringes in electron micrographs is proposed and applied to Cu_3Au and Fe_3Al. The extinction distance ξ_g and the intensity of a g (superlattice) reflexion at the exact $2g$ Bragg position in the systematic condition are calculated as a function of S at various accelerating voltages with the many-beam dynamical theory. In the case of Cu_3Au the variation of ξ_g with S is predicted to be very large in the range 200–1000 kV, and the intensity of the g reflexion decreases with increase of accelerating voltage. In the case of Fe_3Al with a $B2$-type superlattice, on the other hand, S dependence on ξ_g and the intensity of the g reflexion are not sufficient to determine the value of S with high accuracy at around 200 kV, but they are sufficient at around 1000 kV. An experiment on Cu_3Au reproduces the theoretical prediction and indicates that this method is useful for determining the long-range order parameter, especially in local regions.

1. Introduction

Since the critical-voltage effect was found (Nagata & Fukuhara, 1967) and further applied to the accurate determination of the structure factor (Watanabe, Uyeda & Fukuhara, 1968), a number of new applications of dynamical effects in electron diffraction, such as thickness fringes (Ichimiya, Arii, Uyeda & Fukuhara, 1973), as well as the critical-voltage effect, have been proposed and investigated. Stimulated by these successes, Lally, Humphreys, Metherell & Fisher (1972) have proposed the use of the critical-voltage effect to measure the long-range order parameter. However, Sinclair, Goringe & Thomas (1975) have shown that, although most systems in ordered alloys have a reflexion showing a critical voltage of up to 1000 kV, the critical-voltage variation with the long-range order parameter is generally very small.

In this work, a method which determines the long-range order parameter with high accuracy by using thickness fringes instead of the critical-voltage effect is proposed and applied to Cu_3Au and Fe_3Al with $L1_2$ and $B2$ types of superlattices respectively. The variations of the extinction distances are calculated as a function of the long-range order parameter at various accelerating voltages by the many-beam dynamical theory. Experimental investigations on Cu_3Au are also performed in order to assess the practical implications of these calculations.

2. Theory

When the crystal is set at the Bragg position for the second-order reflexion $2g$ in the symmetric Laue case, expressions of the intensities of the g and $2g$ reflexions at a depth t in the crystal along the direction $\mathbf{z}$ perpendicular to the incident crystal surface can be obtained with the three-beam dynamical theory and written as

$$I_g(t)=|\sum_1^3 C_0^{(j)}C_g^{(j)}\exp[2\pi i\gamma_z^{(j)}t]|^2$$
$$=4[C_0^{(1)}C_g^{(1)}]^2\sin^2\pi[\gamma_z^{(1)}-\gamma_z^{(2)}]t, \quad (1)$$

$$I_{2g}(t)=|\sum_1^3 C_0^{(j)}C_{2g}^{(j)}\exp[2\pi i\gamma_z^{(j)}t]|^2, \quad (2)$$

where

$$\gamma_z^{(1)}=(U_{2g}+g^2+B)/4K,$$
$$\gamma_z^{(2)}=(U_{2g}+g^2-B)/4K,$$
$$\gamma_z^{(3)}=-U_{2g}/2K,$$
$$C_0^{(1)}C_g^{(1)}=\frac{2U_g(A+B)}{(A+B)^2+8U_g^2},$$
$$C_0^{(1)}C_{2g}^{(1)}=\tfrac{1}{2}\frac{(A+B)^2}{(A+B)^2+8U_g^2},$$
$$C_0^{(2)}C_g^{(2)}=\frac{2U_g(A-B)}{(A-B)^2+8U_g^2},$$
$$C_0^{(2)}C_{2g}^{(2)}=\tfrac{1}{2}\frac{(A-B)^2}{(A-B)^2+8U_g^2},$$
$$C_0^{(3)}C_g^{(3)}=0,\quad C_0^{(3)}C_{2g}^{(3)}=-\tfrac{1}{2},$$
$$\gamma_z^{(j)}=k_z^{(j)}-K_z,\quad A=U_{2g}-g^2,$$
$$K_z=\sqrt{(K^2-g^2)},\quad B=\sqrt{[(U_{2g}-g^2)^2+8U_g^2]}, \quad (3)$$

and K is the magnitude of the electron wave vector in the crystal after correction of the wavelength change due to the mean crystal potential, and U_h is the hth-order Fourier coefficient of the crystal potential. (1) indicates that oscillations in intensity of the g reflexion will occur with the periodicity of $[\gamma_z^{(1)}-\gamma_z^{(2)}]^{-1}$, which is designated as the extinction distance ξ_g, if t varies. This gives rise to thickness fringes in the wedge-shaped crystal. The extinction distance ξ_g is extremely im-

portant in the dynamical theory of contrast and is a function of U_g and U_{2g}:

$$\xi_g = \frac{2K}{\sqrt{[(U_{2g}-g^2)^2+8U_g^2]}}. \quad (4)$$

The hth-order Fourier coefficient of the crystal potential is related to the crystal structure factor F_h and the Debye–Waller factor $\exp(-M_h)$ by

$$U_h = \left(1+\frac{eE}{m_0c^2}\right)\frac{1}{\pi V_c}\exp(-M_h)F_h, \quad (5)$$

where E and m_0 are the accelerating voltage and electron rest mass. Then, when the g reflexion is a superlattice reflexion and U_{2g} is given, U_g, which is proportional to the long-range order parameter S, can be determined from ξ_g with (4) and (5). Considering that the closer the value of U_{2g} approaches that of g^2, the larger the dependence of ξ_g on U_g becomes, and that U_h is proportional to the incident electron energy, we can select the most convenient accelerating voltage for the determination of the long-range order parameter, S, in various alloys with superlattices.

Stimulated by these predictions, the extinction distance and the intensity of the g reflexion of Cu_3Au and Fe_3Al, which were set at the Bragg position for the $2g$-reflexion in the systematic condition, were calculated by the 11-beam dynamical theory with an electronic computer FACOM 230-75 of the Computer Center, Kyushu University. Here, the 100 reflexion, which is a superlattice reflexion, was taken as g for Cu_3Au and the 200 reflexion for Fe_3Al, and the calculations were performed in the symmetric Laue case. Fig. 1 shows the computed intensities of the g and $2g$ reflexions of Cu_3Au at 200 kV from three-beam [equations (1) to (3)] or 11-beam theory. The scattering factors and the Debye–Waller factors used were those of Doyle & Turner (1968) and Thomas, Shirley, Lally & Fisher (1974) respectively; the absorption effect was neglected. The diffracted intensities I_g and I_{2g} oscillate with depth in the crystal. The depth periodicity of the oscillation and the maximum intensity of each period of each reflexion are not always unique, except those calculated by a three-beam approximation of the g-reflexion [equation (1)], because of the consequence of the many-beam dynamical effect. Here, we define the maximum intensity and the depth periodicity of the first oscillation for an h-reflexion as I_h^{max} and ξ_h respectively. The values of I_{2g}^{max} and ξ_{2g} do not largely depend on the long-range order parameter S, but I_g^{max} and ξ_g largely depend on S. Wave intensity strong enough for observation of the thickness fringes as well as the large dependence of ξ_g on S is required to determine the value of S from thickness fringes in electron micrographs. In Fig. 2 are plotted the value of ξ_g and the ratio of I_g^{max} to incident-beam intensity I_0 as a function of S at several accelerating voltages of Cu_3Au and Fig. 3 shows those of Fe_3Al. In the case of Fe_3Al, S is the long-range order parameter of the $B2$-type superlattice defined by Eguchi, Matsuda, Oki, Kiyoto & Yasutake (1967). In the case of Cu_3Au the variation of

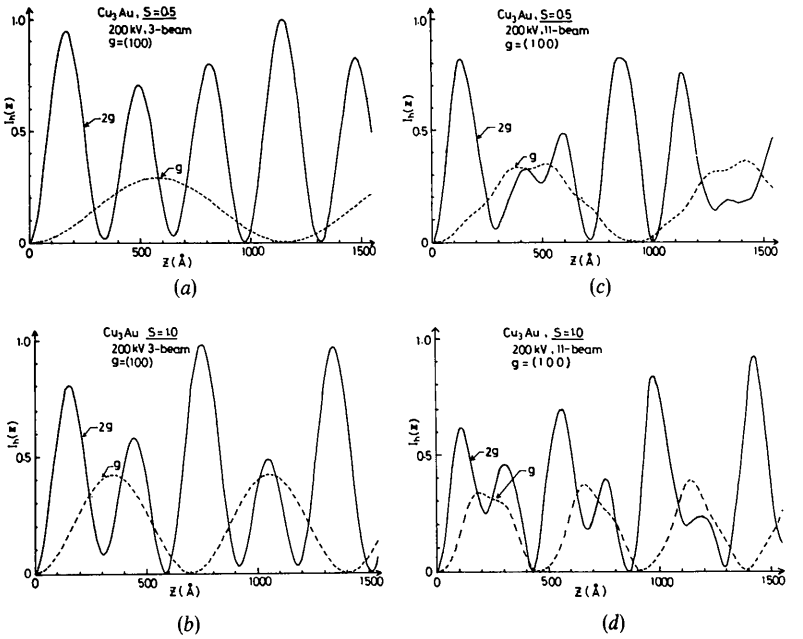

Fig. 1. Theoretical profiles of thickness fringes of g (broken lines) and $2g$ reflexions (solid lines) on Cu_3Au ($L1_2$ type superlattice). (*a*) and (*c*) $S=0.5$. (*b*) and (*d*) $S=1.0$. Lines in (*a*) and (*b*) and those in (*c*) and (*d*) refer to the profiles calculated with three beams and 11 beams, respectively. The crystals are set at the Bragg position for the $2g$ reflexion in the 100 systematic condition.

ξ_g with S is predicted to be very large at 200 through 1000 kV, and the intensity of the g reflexion decreases with increasing accelerating voltage. In the case of Fe_3Al with a $B2$-type superlattice, on the other hand, the S dependence on ξ_g is not sufficiently large to determine the value of S with high accuracy at around 200 kV, but it is large at around 1000 kV. Measurement of ξ_g at the correct accelerating voltage, combined with (4), yields the value of U_g, and hence this method is in principle a highly accurate way of determining the long-range order parameter in various alloys with superlattices. An experiment on Cu_3Au was performed to confirm the theoretical predictions and is described in the next section.

3. Experimental

The specimen of Cu–25 at.% Au was made from 99·99% purity Cu and Au. The required proportions of the materials were melted in an evacuated silica tube in vacuum. After being homogenized at 800 °C for 5 h after cold rolling, the specimens for X-ray experiments were filed down to powder and, for electron microscopy, foil specimens of 0·1 mm thickness were prepared by cold rolling. The foil specimens were sealed in two individual evacuated silica tubes together with the powder specimens and purified He gas. These specimens were slowly cooled from 800 to 376 °C, where they were annealed for 50 h to promote the growth of the ordered domains, and then one specimen was quenched from 376 °C into ice brine and the other was cooled to room temperature at the rate of 2·3 °C h^{-1}. The long-range order parameters for the powdered samples were obtained from the measurement of integrated intensities of X-ray reflexions by the usual method.

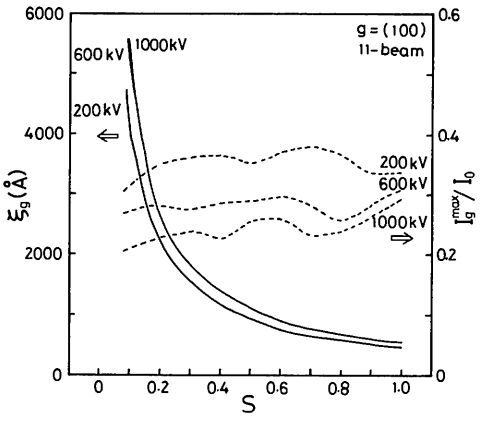

Fig. 2. Theoretical variations of ξ_g (solid lines) and I_g^{max}/I_0 (broken lines) with long-range order parameter S of Cu_3Au at various accelerating voltages. Where ξ_g is the extinction distance of the g reflexion and I_g^{max}/I_0 is the ratio of the maximum intensity of the g reflexion to the incident beam intensity. The crystals are set at the same condition as in Fig. 1.

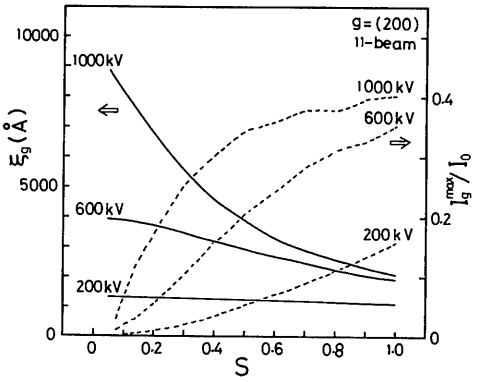

Fig. 3. Same as Fig. 2, but with Fe_3Al. The crystals are set at the Bragg position for the $2g$ reflexion in the 200 systematic condition.

Dark-field micrographs of g and $2g$ reflexions for wedge-shaped specimens at the Bragg position for $2g$ reflexion in the 100 systematic condition were taken at the same magnification. Some of them are shown in Fig. 4, where the thickness fringes and the antiphase domain boundaries can be observed. The thickness fringes are a result of the oscillations of wave intensities. Following the paper written by Hibi, Kambe & Honjo (1955), we interpret the relation between the wave intensities in the crystal and the thickness fringes in the micrograph.

Let a parallel wave enter a wedge-shaped crystal through one surface (incident surface). When Bragg reflexion takes place in the crystal, the intensities of the primary and diffracted waves vary with depth in the crystal as a result of beats between waves, as shown in Fig. 5. The waves then emerge in vacuum as transmitted and diffracted. As the tangential component of each wave-number vector is related continuously on the crystal surface, the thickness fringes in the micrograph are the magnified reproduction of the intensity

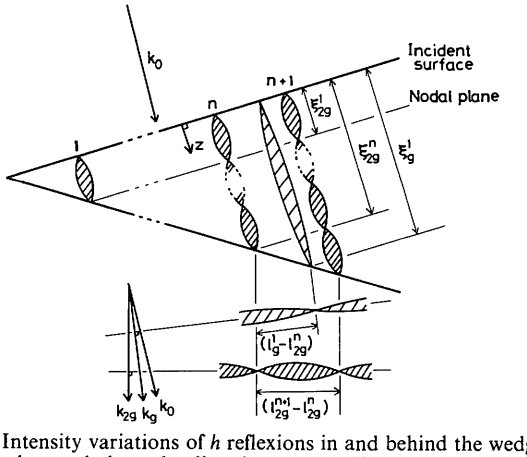

Fig. 5. Intensity variations of h reflexions in and behind the wedge-shaped crystal along the directions perpendicular to the incident surface and h waves. Distances between the nth fringe of the h reflexion and the specimen edge, l^n_h, and between the nodal plane corresponding to this fringe and the incident surface, ξ^n_h, are also shown in the figure.

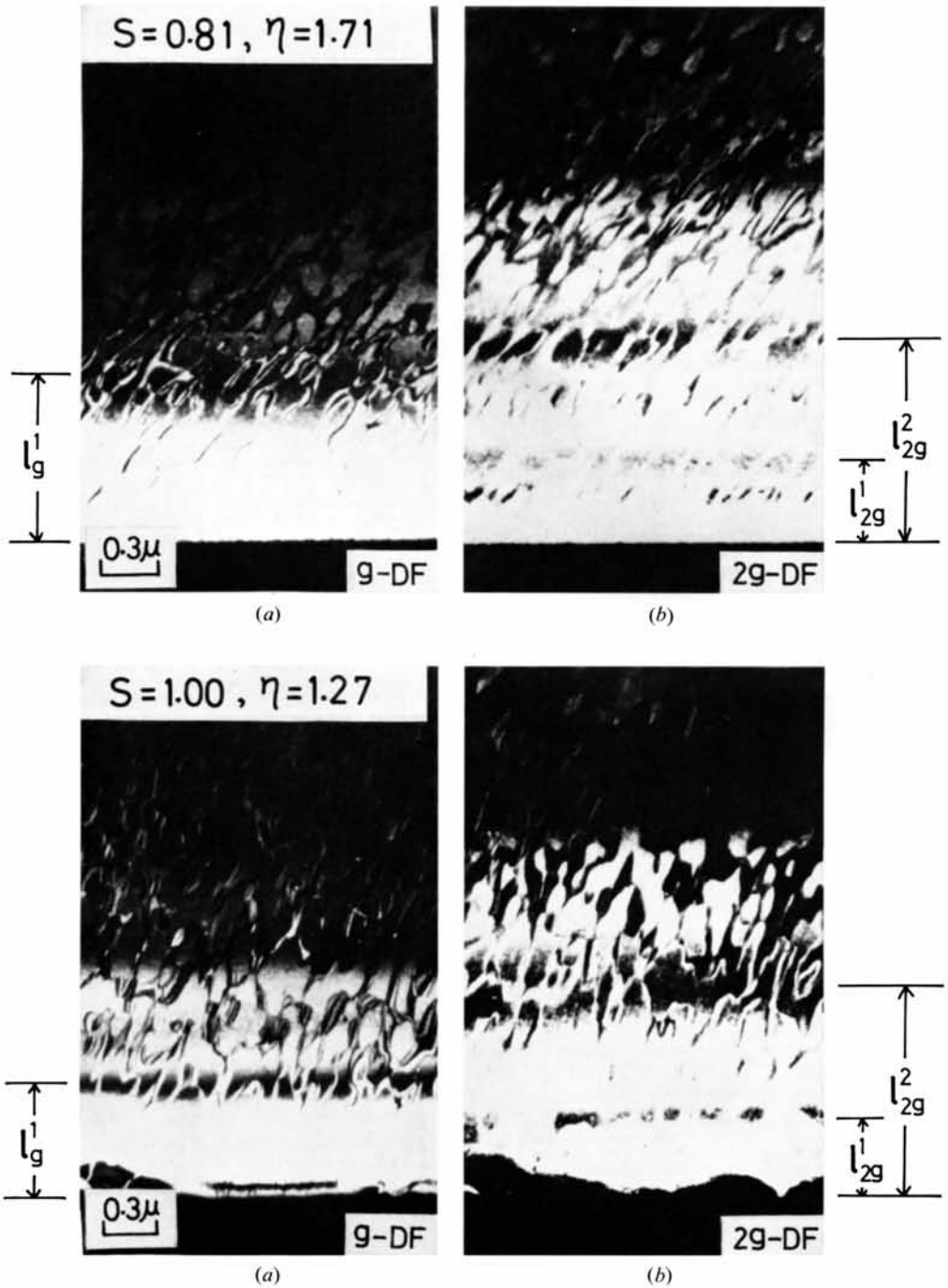

Fig. 4. Electron micrographs showing thickness fringes for the wedge-shaped Cu_3Au specimens of $S=0.81$ and 1.0. (*a*) Dark-field image of the *g* reflexion. (*b*) Dark-field image of the 2*g* reflexion. The specimens are set at same condition as in Fig. 2. The distance of the *n*th fringe of the *h* reflexion from the specimen edge, l_h^n, is indicated in the figure, and will be used later for the comparison with the theoretical prediction. The irregularly curved lines are the antiphase domain boundaries.

[*To face p.* 607

variation within the crystal. In the case of the perfect wedge-shaped crystal the distance, l_h^n, of the nth fringe of the h reflexion from the edge of the crystal, seen in the electron micrograph, is given by

$$l_h^n = \xi_h^n \frac{\cos(\theta_h - \sigma)}{\sin \sigma} \quad (h = 0, g, 2g, \ldots), \tag{6}$$

where ξ_h^n is the distance between the nodal plane corresponding to the nth fringe and the incident surface, θ_h is the angle between the wave-number vector of the h wave and the line normal to the incident surface, and σ is the wedge angle (Miyake, 1974). The value of ξ_h^n can be easily derived from (6) with the observed values of l_h^n, σ and θ_h. But it is difficult to find accurate values of σ and θ_h experimentally.

When the mth node of the g reflexion is between the nth and $(n+1)$th nodes of the $2g$ reflexion, we introduce a new function defined by (7) which is also a function of S;

$$\eta = n + \frac{\xi_g^m - \xi_{2g}^n}{\xi_{2g}^{n+1} - \xi_{2g}^n}. \tag{7}$$

Since $\theta_g \simeq \theta_{2g}$, we notice from (6) and (7) that η can be approximately expressed as follows:

$$\eta = n + \frac{l_g^m - l_{2g}^n}{l_{2g}^{n+1} - l_{2g}^n}. \tag{8}$$

Therefore, η can be obtained experimentally without knowledge of the magnification value and wedge angle of the specimen, and can be compared with the theoretical value. Furthermore, η does not contain the experimental error of l_h^n due to the roundness of the specimen edge.

The observed values of η are shown in Fig. 6, together with the theoretical values, as a function of S determined by X-ray diffraction, where the distances between the first fringes of the g and $2g$ reflexions and between the first and second fringes of the $2g$ reflexion were measured with a photometer. A solid curve and open circles are the values of η obtained theoretically and experimentally, respectively, at the exact Bragg position of the $2g$ reflexion. The error bars indicate the statistical errors of the fringe positions in the micrograph, and contain the error due to the difference in the long-range order parameter in each domain. The error of X-ray measurement is contained within each point. The experiments reproduce the general tendency of the theoretical prediction, although measured values of individual specimens subjected to the same heat treatment are scattered. Sources of scatter in measured values are discussed in the next section together with the systematic deviation of the experimental values from the calculated.

4. Discussion and conclusion

The theoretical treatment developed here is based on the assumption that the specimen is exactly set at the Bragg position for the $2g$ reflexion in the 100 systematic condition, and that the scattering factors of free atoms at rest are applicable for concentrated alloys. These assumptions, together with the shape of the specimen used for electron-microscope observation, will be subjected to the criticism based on the actual experimental conditions.

The two contributions to the error in η, which result from the deviation from the exact Bragg position and the effect of electron-beam heating, are estimated to be less than 0·05 by the calculations for w_{2g} between $-0{\cdot}11$ and 0·14 (w_{2g} is a dimensionless parameter to denote the deviation from the exact Bragg position of the $2g$ reflexion; *i.e.* $w_{2g} = sK/U_{2g}$, where s is the deviation parameter) and for the temperature rise of 100 °C. In the present experiment accuracy better than $|w_{2g}|$ of 0·1 was possible for orientation determinations made *via*

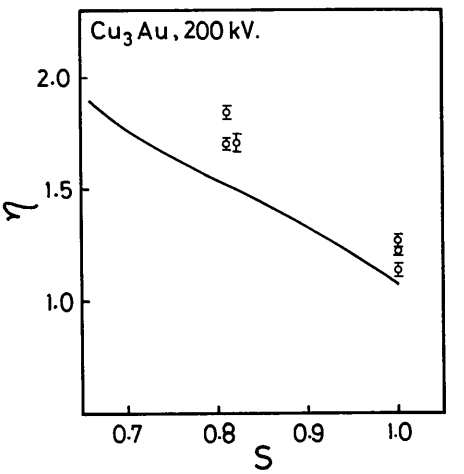

Fig. 6. Variations of η with long-range order parameter S of Cu_3Au. Here, η is given by (7) and (8). The solid line and open circles are the values obtained theoretically and experimentally at the exact Bragg position of the $2g$ reflexion.

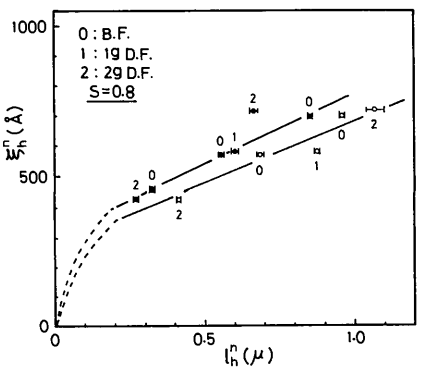

Fig. 7. Thickness variations of two wedge-shaped specimens. The positions of the nodal planes of the h-reflexion, ξ_h^n are plotted against the distances of the corresponding thickness fringes from each specimen edge, l_h^n. Thickness fringes of primary (0), g(1) and 2g(2) reflexions are used. The wedge angles of the specimens are estimated to be 2·55 and 2·97°.

the Kikuchi lines. On the other hand, although great care was taken to avoid the effect of simultaneous reflexions, weak extra fringes appeared in the electron micrographs from some specimens. The effect of weak simultaneous reflexions on the value of η seems to be negligible, although this effect should be studied in more detail.

Transformation of the extinction distance into the thickness fringe is obviously significant only for nearly uniform wedge-shaped specimens, such as cleaved samples, since inaccuracies are introduced when the specimens markedly deviate from wedge-shaped and/or have irregular surfaces and one locally bent. In Fig. 7, the positions of the nodal planes of the h reflexion, which were calculated for $S=0{\cdot}8$ by the 11-beam dynamical theory, are plotted against the distances of the corresponding thickness fringes from the specimen edge in micrographs. We can see in this figure that the specimen shape is considerably different from the uniform wedge shape, and that the main source of scattering is not from the uncertainty of the theoretical prediction, because of the absence of systematic relations between the deviations of the individual specimens. Therefore, irregular surfaces and/or local bending of the wedge-shaped specimen may cause the scattering of the values in Fig. 7 and hence the scattering of η. Systematic deviation of the experimental values from the theoretical in Fig. 6 may be interpreted in terms of the differences between atomic scattering factors of free atoms at rest and those in alloys.

As we have mentioned above, in spite of rather large scattering and systematic deviation of the experimental data from theoretical calculation, relative changes of S can be determined by this method with an experimental error comparable to that by the critical-voltage method in the range of values of S between 0·8 and 1·0. The accuracy can be improved if more perfect wedge-shaped specimens are used.

Furthermore, it should be mentioned that the rate of change of η with S increases as S decreases. Thus we conclude that the thickness-fringe method is useful for determining the long-range order parameter with high accuracy, especially in local regions, if the accelerating voltage is selected so that the rate of change of η with S is maximized. Further experiments on Fe_3Al at various accelerating voltages, 200–1000 kV, are in progress and will be published in the near future.

The fringes due to interfaces such as stacking faults, grain boundaries and antiphase domain boundaries are also related to the structure factor. Utilization of these fringes is another advantageous method of determining the order parameter.

References

DOYLE, P. A. & TURNER, P. S. (1968). *Acta Cryst.* A**24**, 390–397.

EGUCHI, T., MATSUDA, H., OKI, K., KIYOTO, S. & YASUTAKE, K. (1967). *Trans. Japan Inst. Metals*, **8**, 174–179.

HIBI, T., KAMBE, K. & HONJO, G. (1955). *J. Phys. Soc. Japan*, **10**, 35–46.

ICHIMIYA, A., ARII, T., UYEDA, R. & FUKUHARA, A. (1973). *Acta Cryst.* A**29**, 724–725.

LALLY, J. S., HUMPHREYS, C. J., METHERELL, A. J. F. & FISHER, R. M. (1972). *Phil. Mag.* **25**, 321–343.

MIYAKE, S. (1974). *Solid State Phys.* **9**, 136–143 (in Japanese).

NAGATA, F. & FUKUHARA, A. (1967). *Jap. J. Appl. Phys.* **6**, 1233–1235.

SINCLAIR, R., GORINGE, M. J. & THOMAS, G. (1975). *Phil. Mag.* **32**, 501–512.

THOMAS, L. E., SHIRLEY, C. G., LALLY, J. S. & FISHER, R. M. (1974). *High Voltage Electron Microscopy*, Proc. 3rd. Int. Conf., edited by P. R. SWANN, C. J. HUMPHREYS & M. J. GORINGE, pp. 38–47. London and New York: Academic Press.

WATANABE, D., UYEDA, R. & FUKUHARA, A. (1968). *Acta Cryst.* A**24**, 580–581.